Bioengineered 3D Living Fibers as In Vitro Human Tissue Models of Tendon Physiology and Pathology

Isabel Calejo, Claudia J. Labrador-Rached, Manuel Gomez-Florit, Denitsa Docheva, Rui L. Reis, Rui M. A. Domingues,* and Manuela E. Gomes*

Clinically relevant in vitro models of human tissue's health and disease are urgently needed for a better understanding of biological mechanisms essential for the development of novel therapies. Herein, physiological (healthy) and pathological (disease) tendon states are bioengineered by coupling the biological signaling of platelet lysate components with controlled 3D architectures of electrospun microfibers to drive the fate of human tendon cells in different composite living fibers (CLFs). In the CLFs-healthy model, tendon cells adopt a high cytoskeleton alignment and elongation, express tendon-related markers (scleraxis, tenomodulin, and mohawk) and deposit a dense tenogenic matrix. In contrast, cell crowding with low preferential orientation, high matrix deposition, and phenotypic drift leading to increased expression of nontendon related and fibrotic markers, are characteristics of the CLFs-diseased model. This diseased-like profile, also reflected in the increase of COL3/COL1 ratio, is further evident by the imbalance between matrix remodeling and degradation effectors, characteristic of tendinopathy. In summary, microengineered 3D in vitro models of human tendon healthy and diseased states are successfully fabricated. Most importantly, these innovative and versatile microphysiological models offer major advantages over currently used systems, holding promise for drugs screening and development of new therapies.

1. Introduction

Tendons are well-organized and dense connective tissues that respond and adapt to the transmission of contraction forces by muscles to the skeleton, allowing motion and maintenance of posture. As the human lifespan expands and sedentary lifestyle increases, tendon-associated injuries, and pathologies are extremely prevalent leading to patients' disabilities and pain.[1] The hypovascular and hypocellular nature of tendon tissues severely limits their healing capacity and contributes to the loss of functionality and propensity to reinjury.[2] Besides the pain caused by increased neovascularization and inflammation usually seen in tendinopathies,[3] functionality loss is frequently associated with the poor structural organization of collagen fibrils, deposited fibrocartilaginous extracellular matrix (ECM), and increased contents of type III collagen commonly associated with fibrotic tissue formation.[3a,4] Although tendon healing mechanisms follow the common reparative stages consisting of inflammation, proliferation, and remodeling, this process is governed by complex biological factors and cellular crosstalk which are still poorly understood.[5] Remarkably, a major obstacle to the scientific and clinical advancement of tendon therapies is the lack of reliable and valid models to decipher fundamental aspects of tendon physiology and pathology. Despite the low complexity and handling practicability of 2D in vitro culture models, these simple systems cannot accurately recreate the level of complexity stemming from the biophysical, biochemical, and biological cues of native tendon niches.[6] Small animal models (e.g., mouse, rat, rabbit, murine) and ex vivo explant models (e.g., digital flexor tendons,[7] Achilles tendon[8]) which have been widely used to study several processes occurring during tendon pathology and repair in a naturally occurring living environment.[9] Yet, the knowledge that is generated these systems is also associated with numerous limitations. For instance, in the case of animal models, the translation to human clinics is limited by species-specific physiological differences and low accuracy in mimicking the human disease condition,[10] besides the uncontrolled effects of external laboratory microenvironment on animal studies results.[11] On the other hand, difficulties associated with the maintenance of ex vivo tissue homeostasis pose several time-related constraints, indicating that optimization of explant culture conditions are still required for the establishment of a homeostatic baseline in which tendon cells remain quiescent.[6,12] Moreover, because tendon explants are usu-

I. Calejo, C. J. Labrador-Rached, M. Gomez-Florit, R. L. Reis,
R. M. A. Domingues, M. E. Gomes
3B's Research Group
i3Bs—Research Institute on Biomaterials
Biodegradables and Biomimetics
University of Minho
4805-017 Barco, Guimarães, Portugal
E-mail: rui.domingues@i3bs.uminho.pt; megomes@dep.uminho.pt
D. Docheva[+]
Experimental Trauma Surgery
Department of Trauma Surgery
University Hospital Regensburg
Franz-Josef Strauss-Allee 11, 93053 Regensburg, Germany

The ORCID identification number(s) for the author(s) of this article can be found under https://doi.org/10.1002/adhm.202102863

[+]Present address: Department of Musculoskeletal Tissue Regeneration, Orthopaedic Hospital König-Ludwig-Haus, Julius-Maximilians-Univeristy of Würzburg, 97074 Würzburg, Germany

ally obtained from animal tissues,[6] some of the limitations associated with physiological differences among species are also valid for these systems in in vitro modeling. Thus, the development of improved, simplified and less time-consuming platforms to model human tendon physiology and pathology in 3D are still a current need.

In this regard, innovative bioengineered 3D models might be developed using advanced fabrication strategies and bioengineering principles, enabling the mimicry of the native tissue's structure and function.[13] Among the multiple biochemical and biophysical cues of tendon niche, the ECM architecture plays a key role in governing tendon cells behavior, particularly its collagen fiber anisotropic organization. Several works have demonstrated the importance of tendon mimetic topography on stem/stromal cell commitment toward tenogenic phenotype using electrospinning for the tuning of fibers alignment.[14] For example, Schoenenberger et al.,[14c] using commercially electrospun nanofiber mats, demonstrated that cells morphology, phenotype, and matrix turnover were markedly influenced by substrate orientation, favoring a downregulation of the tendon matrix-associated proteins and ECM-remodeling enzymes by cells in contact with random nanofiber scaffolds, opposite to cells in aligned substrates.[14c] Moreover, randomly orientated fibers induced a proinflammatory profile not only in tendon fibroblasts but also in macrophages.[15] Yet, the above studies did not mimicry the hierarchical architecture of tendon tissue, a major feature that should be considered when replicating tendon microenvironment. Plus, beyond the biological signaling resulting from the tissue fibrous structure, tendon cells are embedded in a peri-cellular ECM, which play major roles in their function. This niche is composed of fibrillar and nonfibrillar collagens, important in fibrillogenesis and tendon development,[16] and by noncollagenous components such as elastin, proteoglycans (e.g., decorin), and glycoproteins (e.g., fibronectin, tenascin-c), which provide resistance to mechanical forces, support collagen matrix assembly and regulate cellular processes during tendon development and healing.[17] Strategies such as molecular crowding have been proposed to increase and accelerate ECM deposition in 2D cell cultures, engineering in vitro systems with closer tendon-like matrix.[18] However, the inherent design principle of this concept makes its adaption difficult when fabricating 3D systems that recreate the required biophysical cues of tendon ECM. Therefore, in the present model, platelet lysates (PL) were explored as an interesting bioactive matrix biomaterial for the development of advanced in vitro 3D tendon models. Blood derivatives such PL have attracted great attention as an inexpensive milieu of bioactive molecules (e.g., growth factors, cytokines, adhesion, and structural proteins).[19] Interestingly, several growth factors found in PL components have been related with the maintenance of tendon homeostasis. For example, platelet-derived growth factor (PDGF) has been suggested to be involved in the regulation of tendon cells' fate.[20] One study specifically showed that PDGF immobilized on aligned substrates promoted the tenogenic differentiation of adipose-derived stem cells.[21] Similarly, transforming growth factor-beta (TGF-β) plays central roles in early events of tendon development, tendon neonatal cells recruitment,[22] and tendon cells maintenance.[23] On the other hand, PL is also rich in several structural proteins (e.g., fibrin(ogen) or fibronectin) that are essential as temporary scaffolds

for the first phases of the wound healing process.[19] Recently, the PL composition and intrinsic bioactivity was leveraged to induce the fast cellularization of tissue-engineered constructs,[24] while composite living fibers (CLFs), consisting of sutures cores coated by PL hydrogel laden with human adipose-derived stem cells (hASCs), exhibited a fast deposition of collagen types I and III and great surgical tissue repair potential.[25] Moreover, fibrin gels loaded with a combination of bone morphogenetic protein (BMP)-14, TGF-β3, and VEGF demonstrated enhanced induction of stem cells tenogenic commitment, supporting the notion that multiple biological signaling pathways are involved in the regulation of this mechanism.[26]

So, and building on above-mentioned concepts, we hypothesized that the combination of PL hydrogel coatings with tendon inspired 3D fiber assemblies, would allow the recapitulation of biophysical and biological cues of both healthy and diseased tendon microenvironments. These would allow, at the required throughput and in a time and cost-effective manner, the production of microphysiological systems for in vitro modeling. Thus, in the present study, electrospinning was used for the production of continuous anisotropic and isotropic microfibers threads that were then hierarchically to recreate the hierarchical 3D structure of healthy and diseased tendon fascicles, respectively, while used as core elements of CLFs. Nevertheless, human tendon-derived cells (hTDCs) were selected as the heterogeneous population of stem/progenitor cells and tenocytes found in the native tissue. To fabricate the CLFs, hTDCs were encapsulated within PL hydrogel coatings shells, which replicated the interstitial ECM and constituted a source of growth factors, proteins, and other signaling biomolecules. Furthermore, by combining the proposed concept with 3D printing technologies, we were able to produce large numbers of highly reproducible sample replicates fitting multiwell plate formats in a more time and cost-effective manner. Overall, this unique approach holds great promise for the fabrication of high-throughput 3D in vitro models to study human tendon physiology and pathology, offering a reliable alternative to existing options, opening new avenues in the search for tendon therapies.

2. Results

2.1. Fabrication of a Multiplex In Vitro Platform of Microengineered Tendon Units

The search for physiologically relevant in vitro models enabling high throughput testing is needed not only to study molecular mechanisms and predict preclinical drug efficacy of new therapies in humans, but also to enable the development of improved tissue-engineered constructs for tendon regeneration. To allow an effective mimicry of tendon microenvironment for in vitro modeling, we fabricated a multiplexed system supporting multiple microengineered 3D tendon units fitting standard multiwell plates (**Figure 1**A). The microengineered 3D units were developed to emulate both physiological and pathological tendon microenvironments taking advantage of: 1) the bioinspired topography and architecture of continuous electrospun poly-ϵ-caprolactone (PCL) fiber threads (Figure 1C(i–iv)) to control cell cytoskeleton tension and orientation; and 2) PL coating (Figure 1D) to provide the biological signaling for supporting
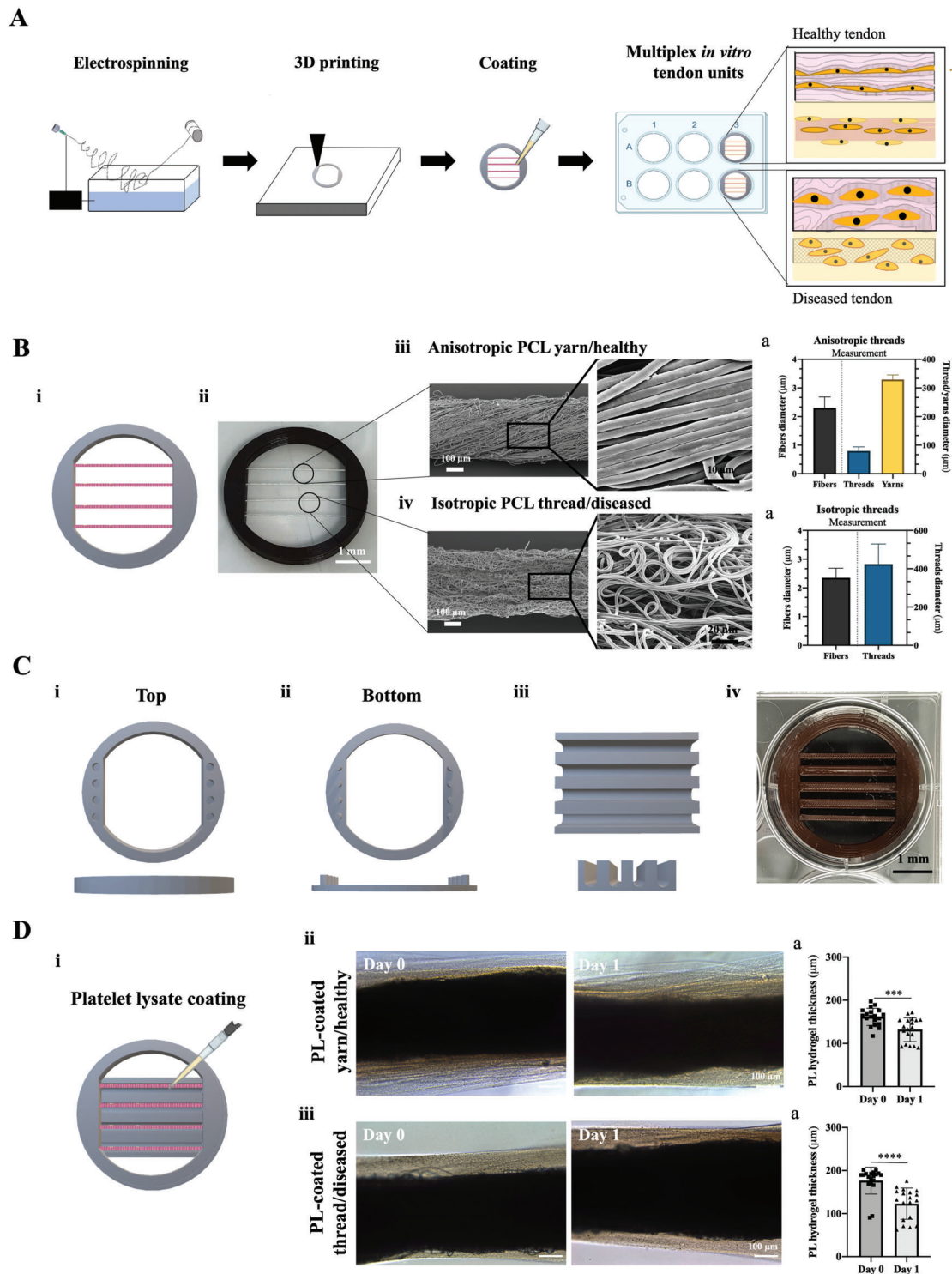
Figure 1. Design of multiplex microengineered 3D in vitro tendon units. A) Schematic illustration of the experimental procedure for the fabrication of 3D healthy and diseased tendon models in vitro. Electrospinning was used for the production of anisotropic and isotropic PCL fiber threads, while the multiplexing platform was printed using a 3D printer. Samples were placed in printed holders and coated with a bioactive hydrogel. B) 3D tendon units were mounted in (i-ii) printed holders and were composed of electrospun (iii) anisotropic yarns (PCL-healthy) and (iv) isotropic threads (PCL-diseased) for physiological and pathophysiological tendon tissue replication, respectively. (a) Measurement of electrospun fibers, threads, and yarns diameter for both anisotropic yarns and isotropic threads. Data are presented as mean ± standard deviation (SD). C) 3D printed holders depicting (i) top, (ii) bottom, and (iii) channels pieces, and (iv) complete structure in 6 well-plates. D) Schematics of (i) platelet lysate (PL) coating and optimized PL-coated (ii) anisotropic yarns (healthy) and (iii) isotropic threads (diseased) at days 0 and 1. Scale bars, 100 μm. a) Hydrogel thickness evaluated in PL-healthy (***, $p = 0.0008$) and PL-diseased (****, $p < 0.00001$) at respective days. Data are presented as mean ± SD ($n = 19$).

**ADVANCED
SCIENCE NEWS**

www.advancedsciencenews.com

**ADVANCED
HEALTHCARE
MATERIALS**

www.advhealthmat.de

hTDCs proliferation and promote fast ECM deposition. The synergy between these biophysical and biological cues is expected to direct hTDCs toward healthy or diseased (fibrotic) phenotypes. Thus, and using a previously customized electrospinning setup,[27] the spinning conditions were first optimized to produce continuous PCL fiber threads with anisotropic and isotropic topographies (Figure S1, Supporting Information), aiming at mimicking the healthy and diseased tendon ECM organization, respectively. Nevertheless, among biopolymers used for electrospinning,[28] PCL was chosen for fibers production as it has been widely used due to its compatibility, mechanical strength, low cost, and solubility in most solvents, and previously demonstrated to enable the production of nanofibers ranging from 92.0 ± 10.0 to 95.0 ± 10.0 nm.[27] Morphometric scanning electron microscopy (SEM) analysis demonstrated that obtained microfiber diameters for both PCL-anisotropic/healthy (Figure 1B(iii),a; 2.30 ± 0.38 µm) and PCL-isotropic/diseased threads (Figure 1B(iv),a; 2.35 ± 0.33 µm) remained within the range of primary collagen fiber, and resembled the microstructural organization of mature human collagen fibrils bundles (fibers) (≈ 1–300 µm).[29] To recreate the tendon's multilevel fibrous architecture, PCL-anisotropic/healthy threads were then hierarchically assembled into yarns (328.6 ± 15.98 µm) with diameters within the range of tendon fascicles (150–1000 µm).[17c] This step was not applied to PCL-isotropic/diseased threads (Figure 1B(iv),a, 444.3 ± 108.7 µm), not only because their dimensions already fell within the targeted fascicle's range, but also because the lower level of hierarchical fiber organization was expected to contribute to a more diseased-like character. Afterward, produced electrospun fiber cores were assembled on a 3D printed system (Figure 1B(i),C(i-ii)). This customized platform consisted of a top part with pillars able to fix the fiber samples when attached to the bottom half (Figure 1C(i-ii)), and a removable multi-basin part, designated as molds, used for hydrogel shells fabrication using low amounts of reagents and biological samples (Figure 1C(iii)). Also, the 3D printed system was designed to fit standard 6 well-plates and to support up to 4 different sample replicates per well (Figure 1C(iv)). Nonetheless, this system can be easily adapted to the specific needs of the user.

Next, to closely replicate tendon ECM and native cellular organization, we fabricated hydrogel shells around produced PCL fibers core. Besides providing a hydrated and soft biodegradable matrix for cell encapsulation while recreating the organization of native tendon fascicles, PL is also a xenofree source of bioactive biomolecules with known roles in tendon healing and regeneration processes that we aimed to explore for the maturation of microengineered CLFs. To induce stable PL gelation and consequent hydrogel formation, the thrombin concentration required to trigger fibrinogen self-assembly[25] and to create a homogenous hydrogel layer was optimized by tuning both thrombin concentration (5 and 10 U mL^{-1}) and incubation times (15–90 min, Figure S2, Supporting Information). Optical microscopy images showed that uniform and homogenous PL hydrogel layers were formed in samples incubated with 10 U mL^{-1} of thrombin for 45 min (Figure 1D(ii-iii)). Additionally, the stability of PL coatings was tested by incubating samples in phosphate-buffered saline (PBS) solution for 1 day (Figure S2, Supporting Information). Although PL shell suffered an expected retraction of $\approx 15\%$ in thickness, as typically seen in this type of soft matrix, it remained stable and well attached to the fiber core. In sum, the multiplex in vitro platform not only assisted in the fabrication and maturation stages of PL-coated fibers allowing an efficient production of CLFs, but simultaneously enabled assay parallelization while providing physical support and easier handling for biological testing.

2.2. Physiological Tendon Microenvironment Replicated In Vitro

Within tendon 3D microenvironment, tendon resident cells play a critical role tissue's function and homeostasis, namely on ECM formation and remodeling.[30] Physiologically, collagen fibrils are produced in cellular recesses, then brought together to form collagen fibril bundles and these are afterward assembled into ordered structures, such as tendon fascicles.[31] Also, tendon cells are reported to influence collagen fibrils orientation, as these can be traced from locations deep within the cell, where they may coexist with numerous shorter fibrils.[31] Moreover, within the tissue, tenocytes present a spindle-shaped morphology and are aligned in the same direction of the dense collagen fibers network.[32] So, when trying to recreate a physiological microenvironment, cells orientation, alignment, and expression of tenogenic-related markers were assessed in the developed model (CLFs-healthy). Nonetheless, gelatin hydrogel coatings were used as reference controls for PL-CLFs (CLFs-control), as this biomaterial has been widely used to replicate the collagenous component of tissue's ECM.[33]

2.2.1. High Uniaxial Cytoskeletal Alignment as Result of Close Contact Guidance in CLFs-Healthy

Taking this into consideration, the performance of the developed model was first evaluated regarding the capacity of CLFs to induce cell contact guidance, which depends on hydrogel shell thickness and cell contact with the core fibers surface. F-actin alignment and nuclei aspect ratio of hTDCs over culture time within CLFs-healthy were used to measure the extent of these effects.

As expected, the cellularized PL hydrogel layer suffered a significant and gradual contraction, mostly occurring over the initial 4 days of culture (Figure S3, Supporting Information). This phenomenon has been described to occur as result of fibrin matrix contraction by pulling forces exerted by encapsulated cells.[24b,34] Also, this effect overcame the limitations of extensive hydrogel retraction providing a gradual and additional support for contact guidance promoted by cell's closer interaction of the fiber's surface topography (**Figure 2**A(i)). In contrast, CLFs-control clearly showed a stable and thick hydrogel layer (day 7: 303.10 ± 54.74 µm; day 28: 338.30 ± 60.87 µm, Figure 2A(ii)) with a dispersed distribution of cells across gel width that was maintained up to 28 days of culture (Figure 2A(ii) – DAPI), resulting in lower cell contact with fibers surface.

To assess the impact of these effects on cell morphology and organization, both cytoskeletal alignment and nuclei aspect ratio of encapsulated cells were investigated up to 28 days of culture. Directionality analysis of hTDCs actin filaments in CLFs-healthy showed that cell cytoskeleton organization followed yarns
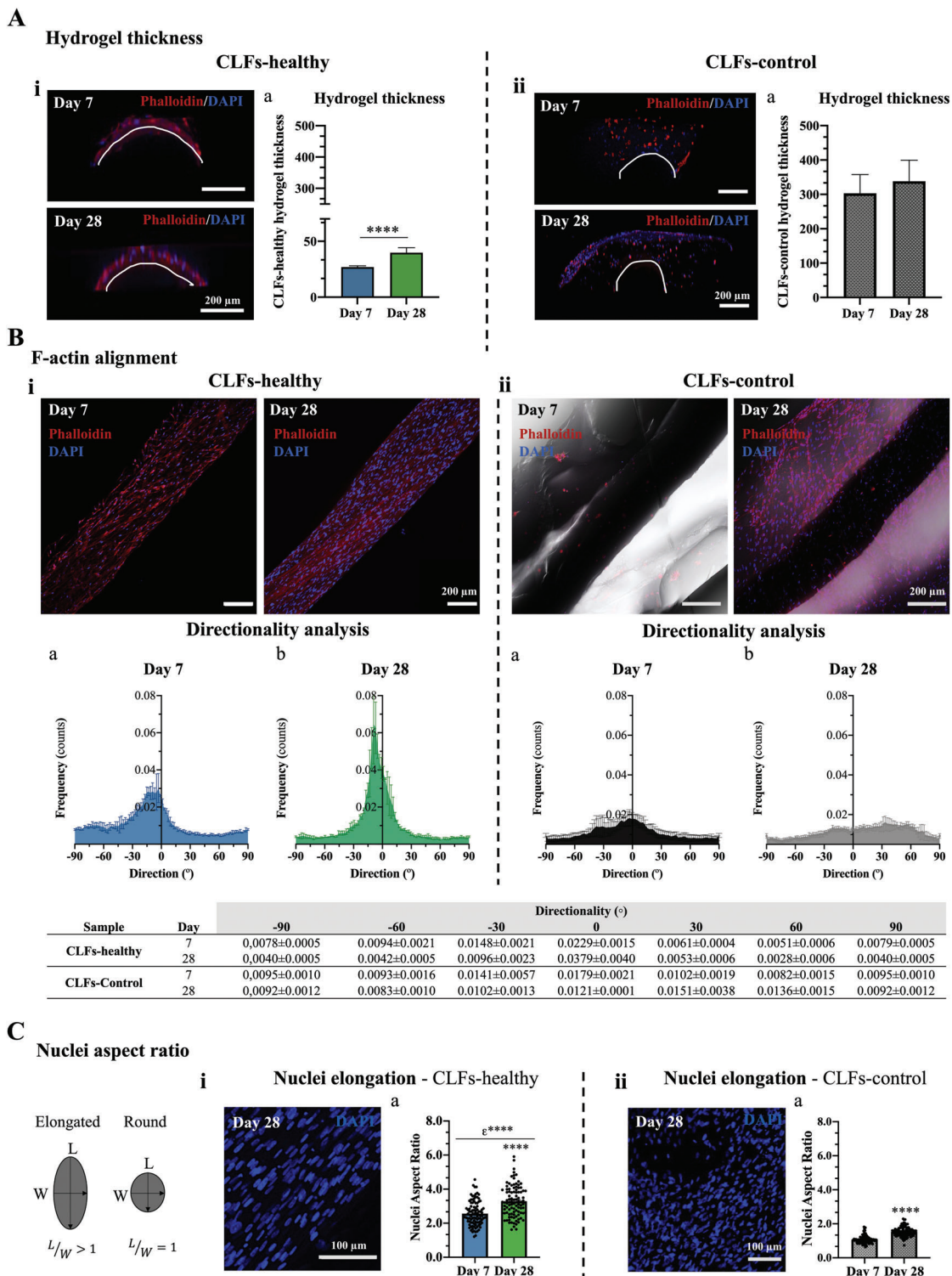
Figure 2. Morphometric analysis of hTDCs encapsulated in CLFs-healthy and CLFs-control. A) Confocal 3D imaging of encapsulated hTDCs in (i) CLFs-healthy and (ii) CLFs-control at 7 and 28 days of culture. White lines represent the interface between the coating and the PCL-yarn core of CLFs. Scale bars, 200 µm. a) Hydrogels thickness measurement at respective days (****, $p < 0.0001$). Data are presented as mean ±SD ($n = 10$). B) Confocal images of hTDCs F-actin filaments (phalloidin, red; DAPI, blue) in (i) CLFs-healthy and (ii) CLFs-control at 7 and 28 days of culture. Scale bars, 200 µm. Directionality analysis for CLFs-healthy and CLFs-control at days a) 7 and b) 28, and respective data table (below). Data are presented as mean ±SD. C) Confocal microscopy images of cell nuclei (DAPI, blue) and a) nuclei aspect ratio of encapsulated hTDCs in (i) CLFs-healthy and (ii) CLFs-control after 28 days of culture. Scale bars, 100 µm. Statistically significant differences between nuclei elongation in CLFs-healthy in comparison with CLFs-control are shown as ϵ****; ****, $p < 0.0001$. Data are presented as mean ±SD ($n = 4$).

**ADVANCED
SCIENCE NEWS**

www.advancedsciencenews.com

**ADVANCED
HEALTHCARE
MATERIALS**

www.advhealthmat.de

topography (Figure 2B(i),a,b), resulting in uniaxially aligned and elongated cells, characteristic of tenocytes embedded within tendon fascicles.[32] In contrast, hTDCs encapsulated within CLFs-control were found to be randomly organized and mainly at the surface of the hydrogel (Figure 2B(ii),a,b). Furthermore, cells in CLFs-healthy show high nuclei aspect ratio after 7 and 28 days (Figure 2C(i)a; 2.56 ± 0.71 and 3.28 ± 0.90 µm, respectively), a phenomena typically correlated with the effective cytoskeletal tension stemming from its pronounced elongation in a preferential axis direction.[35] Opposingly, cells in CLFs-control presented a significantly lower nuclei aspect ratio (1.07 ± 0.23 µm – day 7 and 1.53 ± 0.28 µm – day 28; Figure 2C(ii)a), confirming their less elongated morphology and respective lower cytoskeletal tension.[36] Overall, the obtained results demonstrated that hierarchically assembled PL-CLFs, with different microarchitectures, were able to control cell orientation through contact guidance mechanisms, while simultaneously recreating the organization of native tendon ECM fibrillar structure. These is of major importance when recreating tendon tissue mimetics, as cells have been reported to adapt their phenotypic profile in response to mechanotransduction mechanisms associated biophysical cues from 3D ECM architectures.[27,37]

2.2.2. CLFs-Healthy Support the Expression of Tenogenic-Related Markers and Synthesis of Tenogenic-Rich ECM

The potential of CLFs to support the tenogenic commitment of encapsulated hTDCs was assessed through gene and protein expression analysis of recognized tendon-related markers, tenomodulin (TNMD), scleraxis (SCX), and mohawk (MKX). SCX is a transcription factor expressed during tendon development and differentiation[38] also known to be a positive regulator of tendon differentiation and downstream promoter type I collagen expression,[39] while MKX is a transcription factor described as an important regulator of tendon differentiation.[40] TNMD is a type II transmembrane glycoprotein highly expressed by tenocytes as a regulator of matrix remodeling[41] and shown to be positively regulated by the transcription factor SCX,[42] being a widely accepted marker of mature tendon/ligament lineage.[43] In CLFs-healthy, the transcript levels of *SCX*, *TNMD*, and *MKX* experienced a gradual upregulation from day 0 to day 10 (**Figure** 3A(i)), suggesting a strong healthy tenogenic phenotype. At protein level, TNMD deposition was significantly increased from day 7 to day 28, while SCX was constitutively expressed during culture time (Figure 3A(ii)a,b), indicating the maintenance[44] and maturation[45] of cells tenogenic phenotype when encapsulated in CLFs-healthy. The opposite was observed in CLFs-control, where no differences were found in the deposition of TNMD, while SCX expression was significantly decreased over culture time (Figure S4(iii), Supporting Information), suggesting a possible temporal inhibition of tenogenic phenotype or hTDCs transdifferentiation.

Additionally, the quality of the de novo deposited ECM within CLFs-healthy, was evaluated. For that, we assessed the expression of tendon-related matrix components, specifically collagen type I and III, decorin, tenascin C, and elastin at both gene and protein levels. Collagen type I is the main collagen type found in tendon tissues ECM (≈60–85% dry weight), followed by collagen type III (≈3–5% of total collagen) and noncollagenous matrix components, such as proteoglycans (e.g., decorin) and collagen oligomeric matrix proteins (e.g., lubricin and tenascin C).[4,46] Although collagens type I/ III and tenascin are ubiquitous components of different tissues and not specific markers of tenogenic phenotype, they are often included in tendon markers panels, given their abundance and function in tendon.[47] Moreover, decorin is a proteoglycan highly expressed during tendon development by fibrillogenesis regulation.[48] So, as a first assessment on the impact of encapsulation of hTDCs in CLFs-healthy, real time reverse transcription polymerase chain reaction (RT-PCR) was applied to evaluate the gene expression profile of cells. Transcription levels of collagen type III *(COL3A1)* and decorin *(DCN)* were found to be upregulated at day 10 (Figure 3B(i)), while levels of collagen type I *(COL1A1)* and tenascin c *(TNC)* were continuously expressed during culture time, suggesting that the topography of CLFs-healthy may be inducing a tissue-specific behavior.

This was further confirmed with immunocytochemistry of collagen type I (COL1) and III (COL3), elastin (ELAS), and decorin (DCN), where the expression of tendon ECM-related markers was evident as early as 7 days of culture. Remarkably, after 28 days of culture, cells in CLFs-healthy are embedded in a dense de novo deposited ECM (Figure S5, Supporting Information) that could not be achieved in our previous studies where cells were directly seeded on similar 3D fibrous scaffolds.[27,37b] Furthermore, this ECM was found to be rich in COL1 and DCN (Figure 3B(ii),a–c), while COL3 synthesis decrease over culture time (Figure 3B(ii),b). Interestingly, elastin, an ECM component known for its role in facilitating fascicle sliding and recoil,[49] was also detected in CLFs-healthy (Figure 3B(ii)d). The composition of this newly deposited matrix in CLFs was consistent with the profile described for the ECM of the tendons, where COL1 is the major structural fibrillar protein, and DCN and ELAS have been identified as important components for a proper tendon function.[49a,50]

Overall, obtained results show that the 3D tendon mimetic model composed of anisotropic CLFs in combination with the bioactive PL directed hTDCs response toward a regenerative phenotype, leading to microengineered CLFs exhibiting healthy tendon organotypic profiles and deposition of a teno-like ECM. These key features sustained the hypothesis that the fabricated multiplex 3D tendon units can be an advantageous platform for in vitro human tendon modeling and be considered as an alternative to the currently used tissue explants and/or animal models.

2.3. Pathological-Like Matrix Deposition Associated with Cells Morphological Phenotypic Changes and Unbalanced Matrix Turnover

Bioengineered in vitro models are essential tools not only for investigating the biology of tendon tissues, but as well to study repair and regeneration mechanisms. An important hallmark of chronic tendinopathy or tendon reparative response to an acute injury is the formation of fibrotic scarring tissue characterized by a disorganized tendon matrix showing discontinuous, crimped, and thinned collagen fibers lacking the typical hierarchical structure, and hypercellularity.[4,51] The disorganized topography and
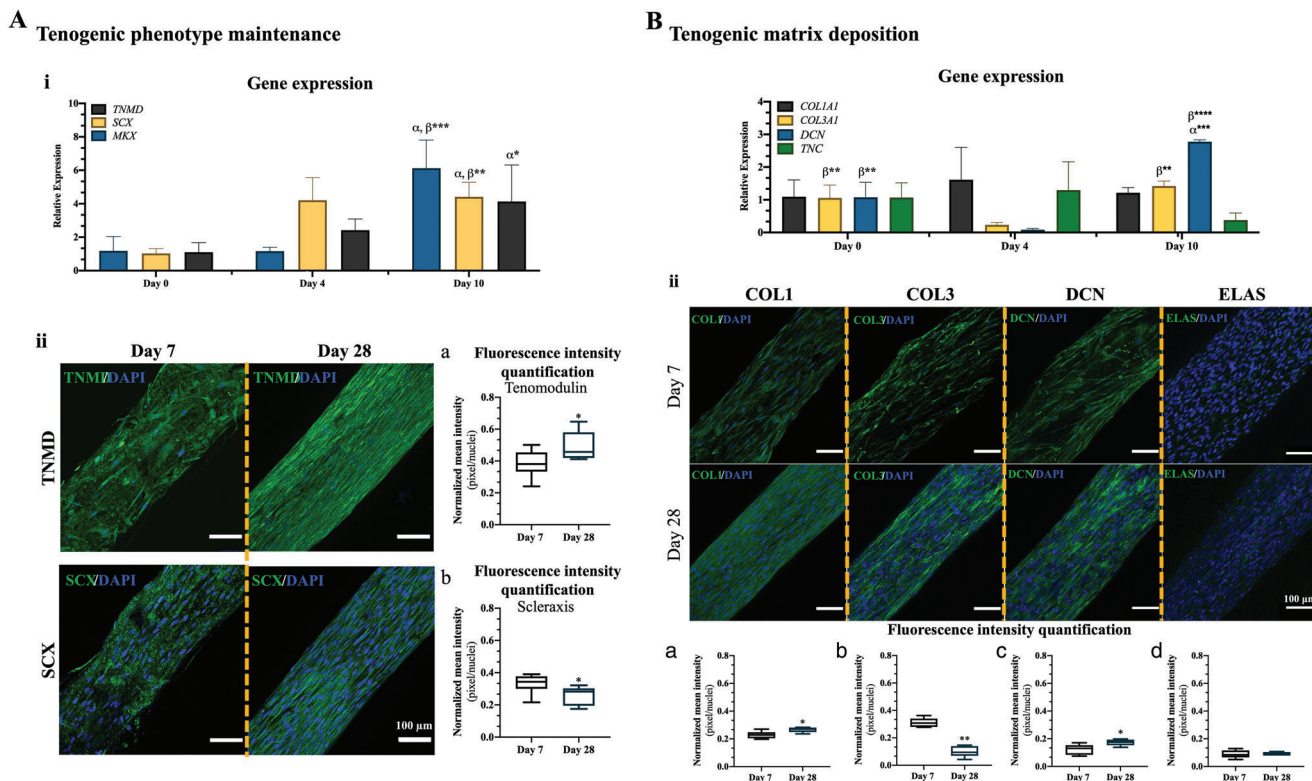
Figure 3. Gene and protein expression of tenogenic markers by hTDCs encapsulated in CLFs-healthy. A) Phenotype maintenance evaluated by (i) gene expression of tenomodulin (*TNMD*; *, $p = 0.028$), b) scleraxis (*SCX*; **, $p = 0.0026$) and c) mohawk (*MKX*; ***, $p = 0.0003$) at 0, 4, and 10 days of culture. Data are presented as mean ± SD ($n = 4$). α and β are statistically significant in comparison with day 0 and day 4, respectively. Expression of target genes was normalized against the average of *ß-actin/YWHAZ* reference genes and gene expression in all conditions was normalized to day 0. (ii) Fluorescence microscopy of tenogenic markers tenomodulin (TNMD) and transcription factor scleraxis (SCX) at 7 and 28 days. Nuclei were counterstained with DAPI. Scale bars, 100 μm. Fluorescence intensity quantification of a) TNMD (*, $p = 0.038$, $n = 6$) and b) SCX (*, $p = 0.026$, $n = 6$) evaluated at 7 and 28 days of culture. B) Matrix deposition assessed by (i) gene expression of collagen type I, alpha chain 1 (*COL1A1*), collagen type III, alpha chain 1 (*COL3A1*; **, $p = 0.0029$; ***, $p = 0.0002$), decorin (*DCN*; **, $p = 0.0029$; ***, $p = 0.0001$; ****, $p < 0.0001$), tenascin (*TNC*), by RT-PCR at 0, 4, and 10 days of culture. Data are presented as mean ± SD ($n = 4$). α and β are statistically significant in comparison with day 0 and day 4, respectively. Expression of target genes was normalized against the average of *ß-actin/YWHAZ* reference genes and gene expression in all conditions was normalized to day 0. (ii) Fluorescence microscopy of ECM-related tenogenic markers, type I collagen (COL1), type I collagen (COL1), decorin (DCN) and elastin (ELAS) at 7 and 28 days. Nuclei were counterstained with DAPI. Scale bars, 100 μm. Fluorescence intensity quantification (bottom) of a) COLI (*, $p = 0.026$, $n = 6$), b) COLIII (**, $p = 0.0022$, $n = 6$), c) DCN (*, $p = 0.022$, $n = 6$), and d) ELAS ($n = 6$) evaluated at 7 and 28 days of culture.

lower hierarchical organization of isotropic threads aim to replicate in vitro the physical cues of these scar tissues.[52] Thus, next we hypothesized that CLFs-diseased would drive hTDCs response toward a fibrotic profile.

2.3.1. Encapsulated hTDCs in CLFs-Diseased Present a Higher Proliferation and Cytoskeleton Misalignment

The fabricated diseased tendon units were first evaluated in terms of hTDCs proliferation and organization. Interestingly, although both CLFs show similar cell densities at day 28, at day 7, cell numbers are significantly higher in the CLFs-diseased than in CLFs-healthy, suggesting a higher initial proliferative activity in these units (**Figure 4**A(i)). This behavior was accompanied by a lower degree of cytoskeleton alignment in cells within CLFs-diseased (Figure 4A(ii)) compared to the CLFs-healthy. Indeed, staining of the cytoskeletal actin filaments at day 7 shows that encapsulated cells were able to migrate without showing a marked

preferential orientation, as supported by the results of f-actin directionality analysis (Figure 4A(ii)a). After 28 days, a small peak is observed in the orientation map, probably associated with cell crowding and high ECM deposition occurring over time, which has been related to a high proliferation occurring during tendon remodeling phase after injury,[53] resulting in cell polarization and leading to some degree of alignment along the fibers.

2.3.2. CLFs-Diseased Induced a Tenogenic Drift Over Culture Time

Afterward, the effect of CLFs-diseased on encapsulated hTDCs phenotype was evaluated at both gene and protein levels. First, the expression of tendon markers was analyzed by RT-PCR (Figure 4B(i)). While cells in CLFs-diseased showed increased *SCX* and *TNMD* transcript levels at day 10, *MKX* transcript levels were found to be decreased with culture time (Figure 4B(i)). Nevertheless, complementary immunocytochemistry imaging quantification revealed an almost absent protein expression of SCX
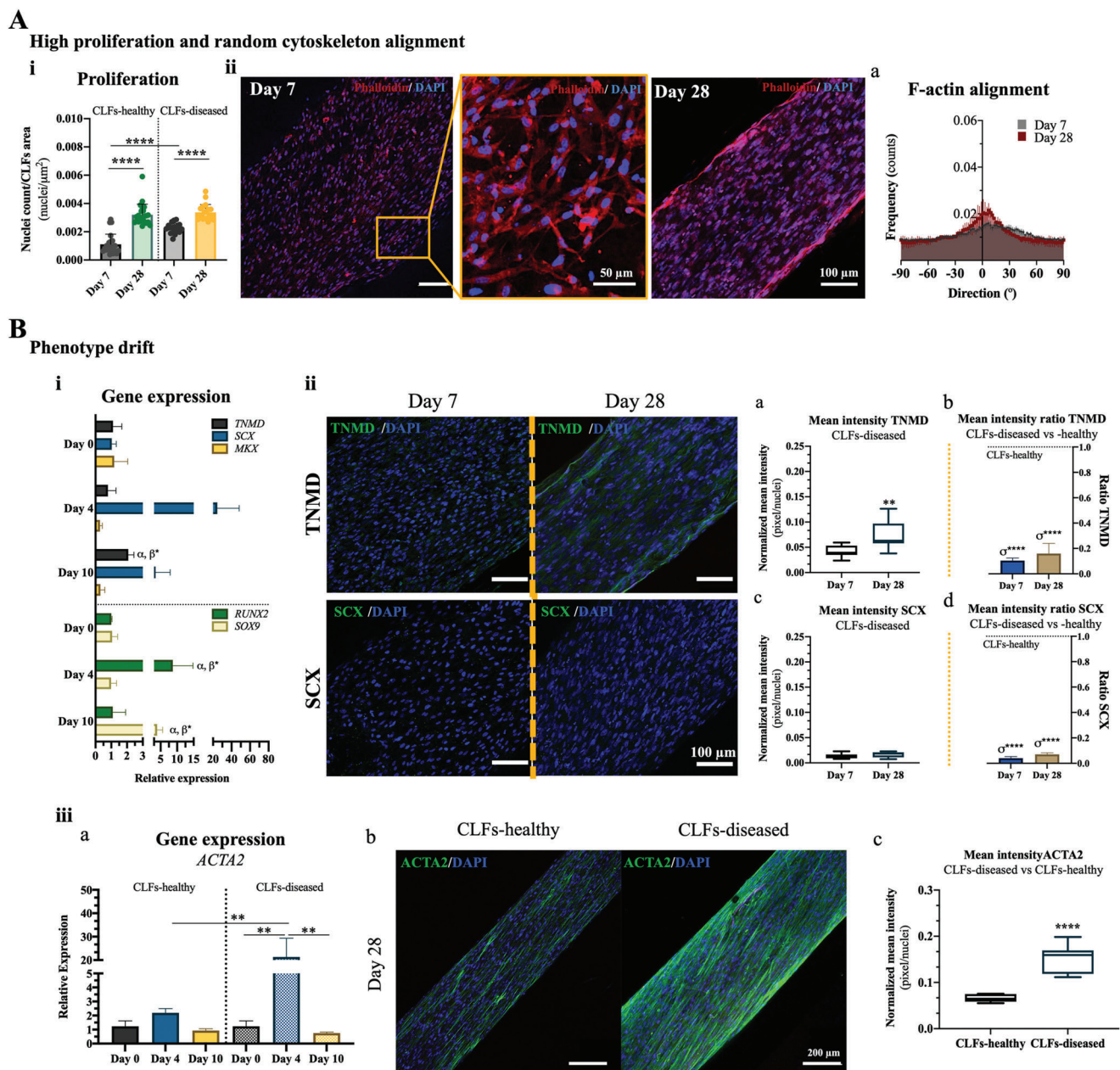
Figure 4. Analysis of proliferation, F-actin alignment and phenotype drift in hTDCs encapsulated in CLFs-diseased. A) Cell's proliferation (i) evaluated at 7 and 14 days of culture in both CLFs-healthy (****, $p < 0.0001$) and CLFs-diseased (****, $p < 0.0001$). (ii) Confocal imaging of nuclei (DAPI, blue) and actin filaments (F-actin, phalloidin, red) staining of encapsulated hTDCs in CLFs-diseased after 7 and 28 days of culture. Scale bars, 100 and 25 µm. a) Directionality analysis of actin filaments orientation for CLFs-diseased at 7 and 28 days. B) Phenotype drift evaluation through (i) gene expression of *TNMD* (*, $p = 0.05$), *SCX*, *MKX*, *RUNX2* (*, $p = 0.05$), and *SOX9* (*, $p = 0.01$) by RT-PCR analysis at 0, 4 and 10 days of culture. Data are presented as mean ± SD ($n = 4$). α and ß are statistically significant in comparison with day 0 and day 4, respectively. Expression of target genes was normalized against the average of *ß-actin/YWHAZ* reference genes and gene expression in all conditions was normalized to day 0. (ii) Fluorescence microscopy of TNMD and SCX at 7 and 28 days. a–c) Fluorescence intensity quantification of respective proteins evaluated at 7 and 28 days of culture ($n = 6$) and b–d) ratio of proteins of interest between CLFs-healthy and CLFs-diseased at both culture times. σ is statistically significant in comparison with the correspondent day in CLFs-healthy. Nuclei were counterstained with DAPI. Scale bars, 100 µm. (iii) Fibrotic myofibroblastic marker evaluation. a) Gene expression of smooth alpha muscle actin (*ACTA2*) at days 0, 4, and 10 in both CLFs-healthy and -diseased (**, $p = 0.009$). Data are presented as mean ± SD ($n = 4$). Expression of target genes was normalized against the average of *ß-actin/YWHAZ* reference genes and gene expression in all conditions was normalized to day 0. b) Confocal images acquired for the expression of smooth alpha muscle actin (ACTA2) at 28 days of culture in CLsF-healthy and CLFs-diseased. Nuclei were counterstained with DAPI. Scale bars, 200 µm. c) Mean intensity quantification (****, $p < 0.0001$) performed for the respective samples ($n = 6$).

ADVANCED
SCIENCE NEWS

www.advancedsciencenews.com

ADVANCED
HEALTHCARE
MATERIALS

www.advhealthmat.de

in CLFs-disease, which was significantly lower compared to the CLFs-healthy (Figure 4B(ii)f). Moreover, although TNMD deposition was significantly increased after 28 days of culture, it showed significantly lower levels compared to CLFs-healthy (Figure 4B(ii)a–c). The absence of these markers has been correlated with a loss or depletion of tendon stem cells' capacity to differentiate into tenocytes and deposit tendon-like ECM,[39,40] contributing to tendinopathies progression.[54] Furthermore, the expression profiles of common osteoblastic and chondrogenic genes, which are usually associated with tenogenic drift/degeneration pathways,[55] were also analyzed. Levels of the osteogenic-related marker runt-related transcription factor 2 (*RUNX2*) were significantly increased at day 4, while levels of the chondrogenic marker SRY-Box transcription factor 9 (*SOX9*)[56] were significantly increased at day 10 compared with both 0 and 4 days of culture (Figure 4B(i)). The expression trend of these two transcription factors is consistent with tendon degeneration associated with detrimental effects on tissue mechanical loading capacity.[57] Moreover, the levels of smooth alpha muscle actin (*ACTA2*), a marker of "myofibroblast" phenotype acquisition associated with tendinopathy and tissue fibrogenesis,[58] were significantly increased after 4 days of culture and also when compared with the levels observed for CLFs-healthy (Figure 4B(iii)), indicating a myofibroblast differentiation/activation and suggesting the commitment of hTDCs toward a fibrotic phenotype.

2.3.3. CLFs-Diseased Induce a Temporal Unbalanced Matrix Turnover Supporting the Deposition of Fibrotic ECM

The pathologic hallmark of tendon fibrosis is underlined by changes in the composition of interstitial ECM.[59] This involves altered deposition of the structural ECM proteins and the expression of metalloproteinases that regulate the biological tissue homeostasis.[60] Thus, gene expression of *COL1A1*, *COL3A1*, *DCN*, and *TNC* was evaluated in CLFs-diseased by RT-PCR (**Figure 5**A(i)). Transcription levels of *COL1A1* and *TNC* were found to be increased at early time points (4 days), suffering a significant downregulation at later culture times. On the other hand, *DCN* levels were decreased after 4 days of culture, whereas an upregulation was observed at later time points (Figure 5A(i)). At protein level, a sustained expression of DCN was observed at both 7 and 28 days of culture in CLFs-diseased (Figure 5A(ii)a), commonly associated with poor matrix organization in tendinopathy.[61] These findings were then correlated with COL1 and COL3 deposition, where it was observed a marked impact over collagens deposition associated with core fiber topography (Figure 5A(iii)). In CLFs-diseased, COL3 was favored against COL1 synthesis (Figure 5A(iii),a), while the opposite has been verified in CLFs-healthy. The differences in the deposition of these two types of collagen resulted in significantly lower COL1/COL3 ratio in CLFs-diseased than in CLFs-healthy, an effect that has been related to the formation of a fibrotic-like tissue.[62] Similar observations also occur in pathologic tendons, which show microscopic irregular fibrillar collagen alignment and molecular changes in collagen composition involving an increased ratio of COL3/COL1.[63] These results, combined with the significantly higher amounts of ACTA2 expressed by hTDCs in CLFs-diseased as previously demonstrated in Figure 4B(iii), point to the depo-

sition of a fibrotic-like matrix in our diseased tendon units. Interestingly, altered collagen microstructure is a known promoter of stromal/stem cells myofibroblast differentiation,[64] a process that is further induced by TGF-β1[65] which is one of the main components of PL.[66]

Matrix metalloproteinases (MMPs) are actively involved in physiological ECM turnover, a critical and continuous process that maintains the healthy state of tendon tissues, contributing to tendon healing and also the progression of tendinopathies.[67] Considering that ECM remodeling is a process dependent on the balanced activity of MMPs and their inhibitors (tissue inhibitors of metalloproteinases, TIMPs), their protein levels were also analyzed in CLFs-diseased and compared to the ones found in CLFs-healthy (Figure 5B; and Table S1, Supporting Information). In the case of CLFs-diseased, significantly higher concentrations of MMP-1 and MMP-9 were observed when compared to CLFs-healthy after 10 days (Figure 5B), proposing an higher degradation of fibrillar collagens (including collagen I) and its fragments.[60] Moreover, MMP-2 and MMP-3, which degrade minor proteins in tendon ECM such as collagen III and proteoglycans,[60] presented decreased levels over culture time in CLFs-diseased when compared to CLFs-healthy (Figure 5B). Nonetheless, MMP-8 levels were continuously decreased over culture time in CLFs-diseased. Considering the key roles that MMPs play on the regulation of ECM composition and turnover, this secretion trend might have contributed to the lower COL1/COL3 ratio seen in CLFs-diseased. Interestingly, obtained results are in good agreement with what is observed after tendon rupture, where a decreased activity of MMP-2, MMP-3, and MMP-8 associated with a higher activity of MMP-1 is described to lead to an enhanced collagen turnover, followed by a deterioration in the quality of the collagen network.[67b,68] In parallel, TIMP1 levels were significantly upregulated in CLFs-diseased and comparatively higher than in CLFs-healthy at day 10 (Figure 5B), possibly contributing to a disease state of fibrotic nature, which is related to lower collagen remodeling and fibrotic-like ECM formation reflected on its low COL1/COL3 ratio.[69]

In summary, our results showed that CLFs-diseased tendon units combined both the biophysical effects from the combination of isotropic topography of fibers and the reparative biological factors of PL coating, to induce a phenotypic drift in hTDCs and deposition of a fibrotic like-ECM. The close recreation of this microenvironment, commonly observed in pathological tendon tissue, suggested that CLFs-diseased might be used as a relevant bioengineered 3D in vitro model for drug screening and new therapies development.

3. Conclusion

In this work, electrospun PCL yarns/threads with well-defined 3D architecture were combined with the structural and biological factors derived from PL to produce microengineered 3D models, aiming at the recreation of physiological and pathological hallmarks of tendon tissue in vitro. Simultaneously, 3D printing was explored to assemble the produced CLFs on easily adaptable supports, allowing a faster generation of 24 reproducible sample replicates fitting 6-well plate formats (4 samples per mold). The superior performance of PL over alternative hydrogel coatings, such as gelatin, was demonstrated by its higher efficacy in
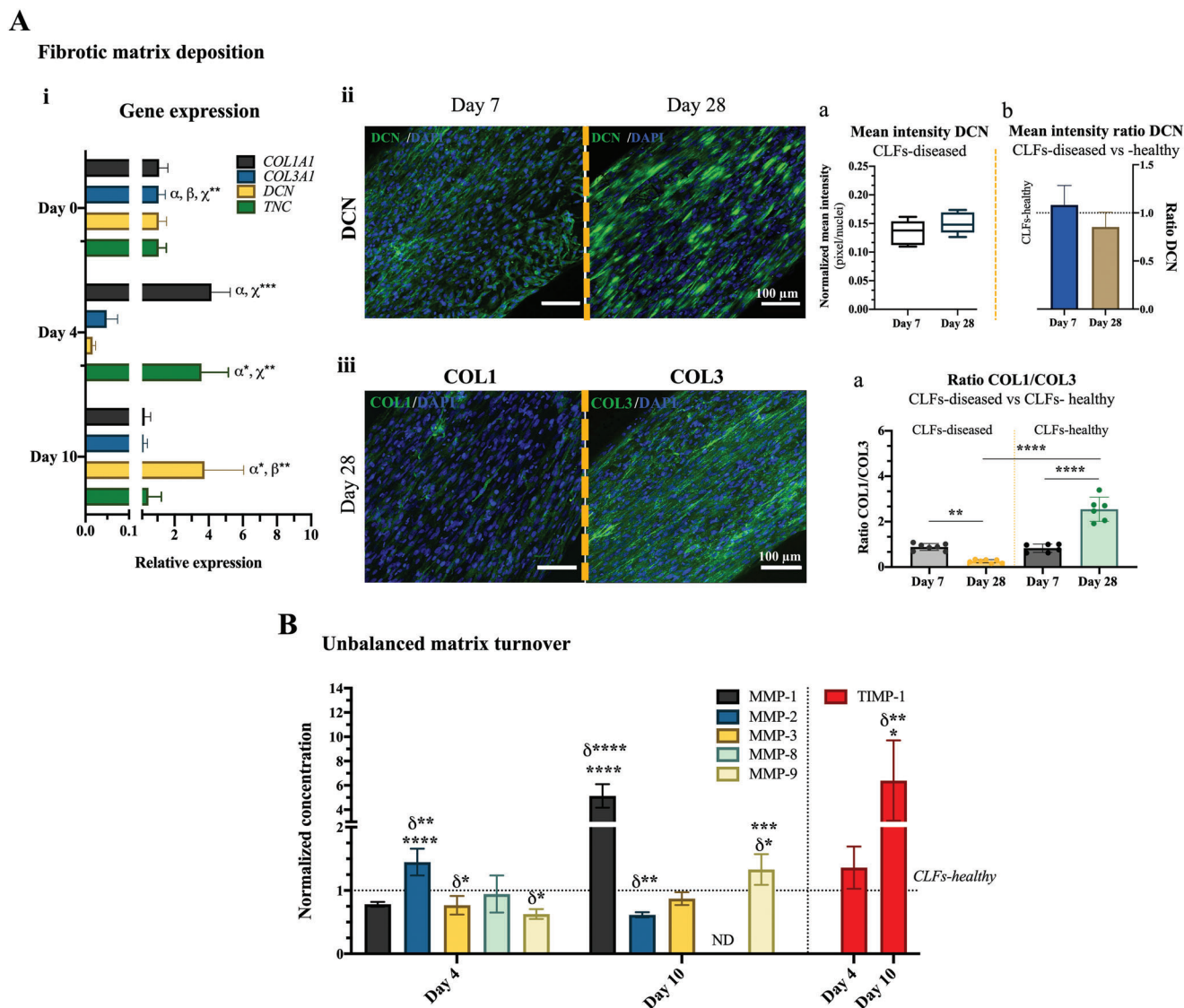
Figure 5. Evaluation of fibrotic matrix deposition and unbalanced matrix turnover in hTDCs encapsulated in CLFs-diseased. A) Matrix deposition assessed by (i) gene expression of *COL1A1* (***, $p = 0.0008$), *COL3A1* (**, $p = 0.003$), *DCN* (*, $p = 0.05$; **, $p = 0.009$), and *TNC* (*, $p = 0.02$; **, $p = 0.006$) by RT-PCR analysis at 0, 4, and 10 days of culture. Data are presented as mean $\pm$ SD ($n = 4$). α, β, and χ are statistically significant in comparison with day 0, day 4, and day 10, respectively. Expression of target genes was normalized against the average of *ß-actin*/*YWHAZ* reference genes and gene expression in all conditions was normalized to day 0. (ii) Fluorescence microscopy of tenogenic-ECM related marker, DCN, a) respective mean fluorescence intensity quantification, and b) DCN ratio between CLFs-healthy and CLFs-diseased at 7 and 28 days of culture ($n = 6$) at 7 and 28 days of culture ($n = 6$). (iii) Confocal imaging of collagen type I (COL1) and collagen type III (COL3) deposition after 28 days. Scale bars, 100 µm. a) COL1/COL3 ratio in CLFs-diseased (**, $p = 0.0022$) versus CLFs-healthy (****, $p < 0.0001$) at 7 and 28 days of culture. Data are presented as mean $\pm$ SD (CLFs-diseased, $n = 7$; CLF-healthy, $n = 6$). B) Unbalanced matrix turnover evaluated through the expression of matrix metalloproteinases-1 (MMP-1; ****, $p < 0.0001$), -2 (MMP-2; **, $p = 0.005$, ****, $p < 0.0001$), -3 (MMP-3; *, $p = 0.03$), -8 (MMP-8), and -9 (MMP-9; *, $p = 0.03$, ***, $p = 0.0002$) and tissue inhibitor of metalloproteinase 1 (TIMP-1; ****, $p < 0.0001$) detected in the extracellular medium of CLFs-diseased. Data were normalized to concentration in CLFs-healthy. δ are statistically significant in comparison with CLFs-healthy at the correspondent day. Data are presented as mean $\pm$ SD ($n = 4$).

promoting cell contact with the topography of core fibers surface, and the induction of hTDCs uniaxially alignment and elongation in CLFs-healthy. Furthermore, CLFs-healthy sustained the expression of tenogenic-related markers while allowing the deposition of a teno-rich ECM, resulting in 3D microphysiological systems with a healthy organotypic profile. In contrast, the CLFs-diseased, based on the same design concept but built on isotropic fiber cores, drove hTDCs response toward a fibrotic profile. This

was reflected in the observed phenotypic drift characterized by the upregulation of nontenogenic related genes, favored deposition of collagen type III over collagen type I, and high expression of myofibroblastic markers. The consequences of this pathogenic profile were also confirmed by the observed unbalanced activity of MMP and TIMP.

Altogether, the proposed concept is a promising strategy for the fabrication of high-throughput micro-engineered 3D in vitro

models of tendon physiology and tendinopathy. This multiplex platform offers a convenient and reliable alternative to existing tendon models with promising application for the discovery of new molecular mechanisms, drug screening, and the development of advanced tendon therapies.

4. Experimental Section

Materials: Poly-ϵ-caprolactone (PCL, average MW 80 000), thrombin from bovine plasma lyophilized powder (40–300 NIH units mg^{-1} protein), gelatin from porcine skin (type A, gel strength ≈300 bloom), PBS, bovine serum albumin (BSA), and phalloidin-tetramethylrhodamine B isothiocyanate were purchased from Sigma-Aldrich (USA). Chloroform was purchased from Honeywell, Switzerland while *N*, *N*'-dimethylformamide (DMF) was purchased from Carlo Erba Reagents (France). Calcium chloride (CaCl$_2$) was purchased from Merk KGaA (Germany). Polylactic acid (PLA) filaments were purchased from Beeverycreative (Portugal). ACTIVA WM transglutaminase was purchased from Ajinomoto (Germany). Ethanol 70% v/v was purchased from AGA (Portugal). Formalin 10% solution neutral buffered was purchased from Bio-Optica (Milano, Italy). Minimum essential medium alpha (α-MEM), Dulbecco's phosphate-buffered saline (DPBS), trypsin-EDTA solution, fetal bovine serum (FBS), antibiotic/antimycotic solution (A/A) were purchased from Life Technologies (USA). Triton X-100 was purchased from ThermoFisher Scientific. 4,6-Diamidino-2-phenyindole dilactate (DAPI) was purchased from VWR (USA). PerfeCTa SYBR Green FastMix and qScript cDNA Synthesis Kit were purchased from Quanta Biosciences (USA). RNeasy Mini Kit (RNA extraction) was purchased from Quiagen (Germany). Hydrogen peroxide 30% w/v was purchased from Panreac Applichem (Barcelona).

Production of PCL Anisotropic and Isotropic Fiber Yarns and Threads: An electrospinning solution was prepared with 17% w/v of PCL dissolved in a chloroform/DMF (v/v, 7:3) solution, and stirred overnight at room temperature (RT). Both anisotropic and isotropic PCL fiber threads were produced using a customized electrospinning setup.[27] Briefly, a syringe with a 21G needle was filled with the PCL in chloroform/DMF solution, and jetted under a constant flow rate of 1.0 mL h^{-1} and voltage of 8.0–9.0 kV, into a 20% v/v ethanol/water bath. Throughout the process, the temperature was maintained at 21–23 °C with a relative humidity of 43–45%. Continuous anisotropic fiber threads were collected with the jetting needle at 16 cm from the surface of the bath by a roller located 20 cm away from the needle at a constant wind speed of 1.09 cm s^{-1}. For isotropic fiber threads, the needle was placed 13 cm above the surface of the bath, the roller was located 13 cm away from the needle, and threads were collected at a constant wind speed of 0.14 cm s^{-1}. Yarns were produced by grouping together 12 anisotropic fiber threads and twisting at 4 turns cm^{-1}, being whereafter denominated as PCL-healthy (anisotropic yarns). Threads with isotropic fibers were no further treated and denominated as PCL-diseased.

Characterization by SEM and Directionality Analysis: Threads topography was characterized using a high-resolution field scanning electron microscope (JSM-6010 LV, JEOL, Japan). Briefly, samples were prepared by placing random pieces of around 1 cm on adhesive carbon films and coated with gold (5–10 nm) under vacuum for 1 min (Cressington, UK) before visualization. Images were collected at an acceleration voltage of 10 kV. ImageJ software was used to measure threads and fiber diameters ($n = 50$). The degree of surface alignment was determined by using directionality analysis applying the Fourier components method within ImageJ software (version 2.1.0/1.43c). For this purpose, scanning electron images were converted to 32-bit images and cropped into three different images. The radial intensities were calculated, and the orientation map was also obtained.

Fabrication of CLFs Support Platform Fitting Multiwell Plates: Customizable 3D polylactic acid (PLA) holders were designed using AutoCAD (version 2019, student license) to hold up to four yarns/threads simultaneously with an approximate length of 2.5 cm. The top and bottom parts were designed with an outer diameter of 3.4 cm and an inner diameter of

3.0 cm to fit into 6-well plates. A pillar-to-hole mechanism was designed to trap yarns/threads between the bottom and top pieces. Moreover, an adjustable bottom piece was designed to separate four CLFs yarns/threads into different channels, presenting a height of 0.5 cm, a diameter of 0.2 cm, and a depth of 0.4 cm. The different parts were 3D printed using B2×300 printer (Beeverycreative, Portugal).

Platelet Lysates and Gelatin Coatings for the Production of CLFs: Platelet lysate (PL) was prepared from platelet concentrates (PC) obtained from healthy human blood donors under a cooperation protocol previously established with Instituto Português do Sangue (IPS; Porto, Portugal), and approved by the Ethical Committee.[25,70] Briefly, PC with a platelet count of one million platelets µL^{-1} were pooled from 80 donors and subjected to three freeze/thaw cycles with liquid nitrogen at −196 and a 37 °C water bath, respectively. These cycles allowed for platelet lysis and protein content release. PL aliquots were then stored at −80 °C. Before use, PL was thawed, and platelet debris was removed by centrifugation at 3000 g for 10 min at RT. Yarns/threads were coated with a hydrogel layer composed of PL. For this purpose, samples were fixed inside the 3D-printed holder and immersed into thrombin solution prepared in 5 × 10^{-3} M CaCl$_2$ at a final concentration of 5 and 10 U mL^{-1} for 15, 30, 45, and 90 min, at RT. Then, a clean multichannel part was placed and filled with equal amounts of fresh PL. Yarns/threads were incubated in PL at 37 °C for 2 h under humidified conditions to allow PL gelation. The morphology of PL hydrogel-coated yarns/threads were analyzed by optical microscopy (DM750, Leica, Schweiz), to observe hydrogel layer formation around yarns/threads core. Herein, four images per sample were acquired immediately after the coating (day 0) and after 24 h (day 1), where PL hydrogel layer thickness was assessed using ImageJ software (version 2.1.0/1.43c). Upon hydrogel optimization, the 45 min incubation time in thrombin solution at a final concentration of 10 U mL^{-1} was selected for subsequent assays.

Enzymatically crosslinked gelatin was prepared according to previously established protocol[71] and used as control hydrogel coatings for the PL-coated structures. Briefly, 5% gelatin from porcine skin (w/v in PBS) was dissolved at 60 °C for 2 h under constant stirring and allowed to cool down to 37 °C. A previously prepared stock solution (20% w/v in PBS) of transglutaminase (100 U g^{-1}) was then thoroughly mixed with the gelatin solution to obtain a 10 U g^{-1} gelatin enzymatic activity. Then, yarns were incubated in gelatin at the same density under humidified conditions for 2 h at 37 °C.

Isolation of Human Tendon-Derived Cells: Tendon tissue was collected from patients undergoing elective orthopedic surgeries at the Hospital da Prelada (Porto, Portugal) under informed consent and according to protocols approved by the Ethical Committee of Hospital da Prelada. Herein, hTDCs were isolated from the sartorius tendon as previously described[72] using three healthy tendon autografts collected from male patients with ages in the range of 25–30 years. Briefly, tissue samples were rinsed in PBS solution containing 10% v/v of A/A. Samples were minced and then digested in 0.1% w/v type I collagenase solution at 37 °C for at least 1 h in an orbital shaker at 200 rpm. Following filtration (100 µm filter) and double centrifugation at 4 °C for 5 min each cycle at 1250 rpm, the supernatant was discarded, and the cell pellet was resuspended in α-MEM. Cells were incubated in standard humidified conditions of 5% CO$_2$ at 37 °C until confluency, where media was removed, and cells were washed with PBS and trypsinized before adding fresh media for cell counting. A portion of counted cell suspension was transferred to a new treated culture flask with fresh media and returned to the incubator. Culture medium was changed every 2–3 days, while splitting protocol was repeated at confluency for cell maintenance. Cells were used at passages 3–4.

Encapsulation in PL and Gelatin (GEL) Hydrogels: Previously produced anisotropic yarns (PCL-healthy) and isotropic threads (PCL-diseased) were placed in the 3D-printed holders. Holders with four sample replicate each were placed in 6-well plates and sterilized by immersion in 70% v/v ethanol for 30 min followed by two washes with sterile DPBS for 30 min. Afterward, yarns/threads were preincubated in a solution of thrombin (10 U mL^{-1}) in calcium chloride (5 × 10^{-3} M) for an optimized time of 45 min at RT. Following preincubation, yarns/threads were incubated with a solution of hTDCs in PL at a density of 2.5 × 10^5 cells mL^{-1} (200 µL per sample) under humidified conditions for 2 h at 37 °C. In the case of cells seeded in

**ADVANCED
SCIENCE NEWS**

www.advancedsciencenews.com

**ADVANCED
HEALTHCARE
MATERIALS**

www.advhealthmat.de

enzymatically crosslinked gelatin, the prepared solution of transglutaminase and gelatin was added to a pellet of 2.5×10^5 cells mL^{-1}, immediately distributed to yarns, and incubated under humidified conditions for 2 h at 37 °C. After incubation, templating molds for CLFs coatings were removed and fresh α-MEM was added. CLFs were transferred to new 6-well plates after 24 h upon seeding and the medium changed every 2–3 days. Non-seeded yarns were used as blanks. Encapsulated hTDCs in PL-coated and GEL-coated yarns were thereafter called as CLFs-healthy and CLFs-control, respectively, while encapsulated cells in PL-coated threads were denominated as CLFs-diseased.

Cell Morphology, Cytoskeleton Organization, and Proliferation Analysis: Actin filaments of cell cytoskeleton were stained with phalloidin at 7 and 28 days of culture. Briefly, samples were washed three times with PBS after formalin fixation and incubated with phalloidin solution for 1 h at RT. Then, samples were washed with PBS and analyzed by confocal laser scanning microscopy (Leica TCS SP8, Microsystems, Wetzlar, Germany). The degree of actin filament alignment was determined through directionality analysis using the Fourier components method using ImageJ software (version 2.1.0/1.43c), as previously described. For nuclei counterstaining, samples were incubated with 4′,6-diamidino-2-phenylindole (DAPI, 1:1000) for 15 min at room temperature. Nuclei aspect ratio was determined by measuring nuclei length and width of at least 100 nuclei in different labeled images of each sample, using ImageJ software (version 2.1.0/1.43c). The length was divided by the width to obtain the correspondent aspect ratio.

For proliferation, the number of nuclei per area of CLFs was calculated. Briefly, blue channel images corresponding to DAPI staining were thresholded, and then the particle analyzer plugin of ImageJ was used to count nuclei numbers. The area of CLFs was measured using ImageJ. Afterward, the number of nuclei divided by the area and the proliferation obtained.

Immunocytochemistry of Coated CLFs-Healthy/Diseased: Samples ($n = 4$) were rinsed with PBS and fixed with 10% formalin at days 7 and 28 after hTDCs encapsulation. After thorough washing with PBS, cellular membranes were permeabilized with 0.1% Triton X-100 in PBS for 20 min at RT. Following washing steps, samples were blocked with 1% BSA in PBS for 30 min. Then, cells were incubated overnight with primary antibodies against anticollagen type I (COL1, ab90395, 1:50), anticollagen type III (COL3, ab175404, 1:100), antidecorin (DCN, ab7778, 1:100), antiscleraxis (SCX, ab58655, 1:200), and antielastin (ELAS, E4013, 1:500) diluted in 0.1% BSA in PBS at 4 °C. The rabbit polyclonal antitenomodulin (TNMD, 1:200) antibody, generated against TNMD C-terminus (237-317 aa) was kindly provided by Prof. Denitsa Docheva (produced in co-operation with Metabion International, Planegg, Germany PAB 201603-00002). Samples were afterward rinsed in PBS and incubated for 15 min with 30% hydrogen peroxide. After PBS rinsing, samples were incubated for 1 h at RT with the respective Alexa Fluor 488 secondary antibodies. Finally, nuclei were counterstained with DAPI for 30 min at RT. Immunolabeled samples were analyzed through confocal laser scanning microscopy and image acquisition settings of each protein marker were maintained constant for results consistency. Expression of proteins of interest was quantitatively analyzed and normalized by cell nuclei number at 7 and 28 days of culture. Briefly, images from established day were split into 3 channels (blue, green, and red). The fluorescence intensity of the green channel corresponding to the protein of interest was measured in several images ($n > 6$) acquired from the different sample replicates. Image's thresholding was performed to separate the signal from the background. Blue channel images corresponding to DAPI staining were thresholded and then the particle analyzer plugin of ImageJ was used to count nuclei numbers. Afterward, the mean fluorescence intensity of each protein marker was normalized by the corresponding number of nuclei and results expressed as normalized mean intensity.

CLFs Hydrogel Thickness: Confocal 3D transversal fluorescence images were acquired for both CLFs-healthy and CLFs-control using confocal laser scanning microscopy (Leica TCS SP8, Microsystems, Wetzlar, Germany). For hydrogel thickness measurement, the fluorescence intensity of blue (DAPI) and red (Phalloidin) channels were split into two separate channels. Afterward, the thickness of hydrogels was measured using the red channel by evaluating the distance between the surface of the core fiber and the hydrogel's edge using ImageJ. Several images ($n > 3$) from different sample replicates were measured.

mRNA Extraction and RT-PCR: Total mRNA was extracted from PL-yarns/threads (healthy/diseased) at days 0, 4, and 10 using RNeasy Mini Kit, according to the manufacturer's instructions. RNA quantity and purity were determined with a NanoDrop spectrophotometer (ND-1000, ThermoScientific, USA). The cDNA synthesis was performed with the qScript cDNA Synthesis kit and using the Mastercycler Realplex (Eppendorf, Germany). Transcript's quantification was carried out by quantitative polymerase chain reaction (qPCR) using the PerfeCTA SYBR Green FastMix kit following the manufacturer's protocol, in a Real-Time Mastercycler Realplex thermocycler (Eppendorf, Germany). Primer sequences (Table S2, Supporting Information) were designed using the Primer-BLAST tool and synthesized by Eurofins Genomics. The evaluation of the relative expression level was performed using the $2^{-\Delta\Delta Ct}$ method. Transcript levels of selected genes were analyzed and normalized to the expression of the selected reference genes, ß-actin (*ACTB*) and Tyrosine 3-Monooxygenase/Tryptophan 5-Monooxygenase Activation Protein Zeta (*YWHAZ*), due to stability of their expression across the sample sets. All values were first normalized against the average value of reference genes transcript values, and then to the transcript values of hTDCs at day 0. Samples were collected and analyzed in quadruplets.

Multiplex Immunoassay: Multianalyte profiling in the supernatant of healthy and diseased CLFs was performed using the Luminex MagPix system (Luminex, Austin, TX). Concentrations of matrix metalloproteinase (MMP)-1, 2, 3, 8, 9, and 13, as well as tissue inhibitor of metalloproteinases (TIMP)-1 were measured using a custom ProcartaPlex human magnetic assay (ThermoFisher Scientific, Austria). The assay was performed as instructed by the manufacturer. The concentration of each analyte was calculated using the Luminex xPONENT 4.2 software. Data are plotted as mean $\pm$ standard deviation where $n = 4$ for each timepoint.

Statistical Analysis: Statistical analysis of data was performed using GraphPad PRISM version 8.4.0. Results were presented as mean $\pm$ standard error of the mean (SD) when not stated otherwise. One-way and two-way analysis of variance (ANOVA) were performed in normally distributed populations followed by Tukey post hoc test for multiple comparisons, whereas the Kruskal–Wallis nonparametric test was performed unless specified otherwise. Nonparametric tests were performed using the Mann–Whitney test. Differences between experimental groups were considered significant with a confidence interval of 95%, whenever $p < 0.05$.

Supporting Information

Supporting Information is available from the Wiley Online Library or from the author.

Acknowledgements

Conflict of Interest

The authors declare no conflict of interest.

Data Availability Statement

The data that support the findings of this study are available from the corresponding author upon reasonable request.

Keywords

3D multiplex models, composite living fibers, in vitro models, tendons, tissue engineering

[1] S. Steinmann, C. G. Pfeifer, C. Brochhausen, D. Docheva, *Int. J. Mol. Sci.* **2020**, *21*, 844.

[2] C. F. Liu, L. Aschbacher-Smith, N. J. Barthelery, N. Dyment, D. Butler, C. Wylie, *Tissue Eng., Part B* **2011**, *17*, 165.

[3] a) N. L. Millar, G. A. Murrell, I. B. McInnes, *Nat. Rev. Rheumatol.* **2017**, *13*, 110; b) S. S. Nikolaeva, Y. A. Khoroshkov, V. A. Dubinskaya, *Bull. Exp. Biol. Med.* **1981**, *92*, 1115.

[4] N. L. Millar, K. G. Silbernagel, K. Thorborg, P. D. Kirwan, L. M. Galatz, G. D. Abrams, G. A. C. Murrell, I. B. McInnes, S. A. Rodeo, *Nat. Rev. Dis. Primers* **2021**, *7* (1):.

[5] P. Sharma, N. Maffulli, *JBJS* **2005**, *87*, 187.

[6] S. L. Wunderli, U. Blache, J. G. Snedeker, *Connect. Tissue Res.* **2020**, *61*, 262.

[7] G. Fessel, J. Cadby, S. Wunderli, R. van Weeren, J. G. Snedeker, *Acta Biomater.* **2014**, *10*, 1897.

[8] Y.-T. Wu, Y.-T. Wu, T.-C. Huang, F.-C. Su, I. M. Jou, C.-C. Wu, *J. Orthop. Transl.* **2020**, *23*, 113.

[9] M. W. Hast, A. Zuskov, L. J. Soslowsky, *Bone Joint Res.* **2014**, *3*, 193.

[10] M. A. Brehm, L. D. Shultz, J. Luban, D. L. Greiner, *J. Infect. Dis.* **2013**, *208*, S125.

[11] E. J. Chesler, S. G. Wilson, W. R. Lariviere, S. L. Rodriguez-Zas, J. S. Mogil, *Neurosci. Biobehav. Rev.* **2002**, *26*, 907.

[12] T. Stauber, U. Blache, J. G. Snedeker, *Matrix Biol.* **2020**, *85–86*, 68.

[13] C. Mota, S. Camarero-Espinosa, M. B. Baker, P. Wieringa, L. Moroni, *Chem. Rev.* **2020**, *120*, 10547.

[14] a) Z. Yin, X. Chen, J. L. Chen, W. L. Shen, T. M. Hieu Nguyen, L. Gao, H. W. Ouyang, *Biomaterials* **2010**, *31*, 2163; b) Z. Yin, X. Chen, H.-x. Song, J.-j. Hu, Q.-m. Tang, T. Zhu, W.-l. Shen, J.-l. Chen, H. Liu, B. C. Heng, H.-W. Ouyang, *Biomaterials* **2015**, *44*, 173; c) A. D. Schoenenberger, J. Foolen, P. Moor, U. Silvan, J. G. Snedeker, *Acta Biomater.* **2018**, *71*, 306.

[15] A. D. Schoenenberger, H. Tempfer, C. Lehner, J. Egloff, M. Mauracher, A. Bird, J. Widmer, K. Maniura-Weber, S. F. Fucentese, A. Traweger, U. Silvan, J. G. Snedeker, *Biomaterials* **2020**, *249*, 120034.

[16] a) D. E. Birk, J. M. Fitch, J. P. Babiarz, K. J. Doane, T. F. Linsenmayer, *J. Cell Sci.* **1990**, *95*, 649; b) C. C. Banos, A. H. Thomas, C. K. Kuo, *Birth Defects Res., Part C* **2008**, *84*, 228.

[17] a) J. A. Martin, D. Mehr, P. D. Pardubsky, J. A. Buckwalter, *Biorheology* **2003**, *40*, 321; b) L. Jozsa, M. Lehto, P. Kannus, M. Kvist, A. Reffy, T. Vieno, M. Järvinen, S. Demel, E. Elek, *Acta Orthop. Scand.* **1989**, *60*, 469; c) P. Kannus, *Scand. J. Med. Sci. Sports* **2000**, *10*, 312.

[18] a) P. Kumar, A. Satyam, X. Fan, E. Collin, Y. Rochev, B. J. Rodriguez, A. Gorelov, S. Dillon, L. Joshi, M. Raghunath, A. Pandit, D. I. Zeugolis, *Sci. Rep.* **2015**, *5*, 8729; b) D. Tsiapalis, A. De Pieri, K. Spanoudes, I. Sallent, S. Kearns, J. L. Kelly, M. Raghunath, D. I. Zeugolis, *Biofabrication* **2020**, *12*, 025018.

[19] B. B. Mendes, M. Gómez-Florit, P. S. Babo, R. M. Domingues, R. L. Reis, M. E. Gomes, *Adv. Drug Delivery Rev.* **2018**, *129*, 376.

[20] A. L. Titan, M. T. Longaker, *Nat. Cell Biol.* **2019**, *21*, 1466.

[21] S. K. Madhurakkat Perikamana, J. Lee, T. Ahmad, E. M. Kim, H. Byun, S. Lee, H. Shin, *Biomaterials* **2018**, *165*, 79.

[22] D. A. Kaji, K. L. Howell, Z. Balic, D. Hubmacher, A. H. Huang, *eLife* **2020**, *9*, e51779.

[23] G.-K. Tan, B. A. Pryce, A. Stabio, J. V. Brigande, C. Wang, Z. Xia, S. F. Tufa, D. R. Keene, R. Schweitzer, *eLife* **2020**, *9*, e52695.

[24] a) B. B. Mendes, M. Gómez-Florit, A. G. Hamilton, M. S. Detamore, R. M. A. Domingues, R. L. Reis, M. E. Gomes, *Biofabrication* **2019**, *12*, 015012; b) B. B. Mendes, M. Gómez-Florit, R. A. Pires, R. M. A. Domingues, R. L. Reis, M. E. Gomes, *Nanoscale* **2018**, *10*, 17388.

[25] R. Costa-Almeida, I. Calejo, R. Altieri, R. M. A. Domingues, E. Giordano, R. L. Reis, M. E. Gomes, *Biomed. Mater.* **2019**, *14*, 034104.

[26] a) M. Bottagisio, S. Lopa, V. Granata, G. Talò, C. Bazzocchi, M. Moretti, A. Barbara Lovati, *Differentiation* **2017**, *95*, 44; b) I. Rajpar, J. G. Barrett, *J. Tissue Eng.* **2019**, *10*, 2041731419848877.

[27] M. Laranjeira, R. M. A. Domingues, R. Costa-Almeida, R. L. Reis, M. E. Gomes, *Small* **2017**, *13*, 1700689.

[28] L. Y. C. Madruga, M. J. Kipper, *Adv. Healthcare Mater.* **2022**, *11*, 2101979.

[29] a) F. H. Silver, Y. P. Kato, M. Ohno, A. J. Wasserman, *J. Long-Term Eff. Med. Implants* **1992**, *2*, 165; b) F. H. Silver, J. W. Freeman, G. P. Seehra, *J. Biomech.* **2003**, *36*, 1529.

[30] a) M. Benjamin, E. Kaiser, S. Milz, *J. Anat.* **2008**, *212*, 211; b) M. O'Brien, *Scand. J. Med. Sci. Sports* **1997**, *7*, 55.

[31] a) E. G. Canty, K. E. Kadler, *J. Cell Sci.* **2005**, *118*, 1341; b) M. Franchi, A. Trirè, M. Quaranta, E. Orsini, V. Ottani, *Sci. World J.* **2007**, *7*, 404.

[32] C. M. McNeilly, A. J. Banes, M. Benjamin, J. R. Ralphs, *J. Anat.* **1996**, *189*, 593.

[33] A. B. Bello, D. Kim, D. Kim, H. Park, S.-H. Lee, *Tissue Eng., Part B* **2020**, *26*, 164.

[34] I. Calejo, R. L. Reis, R. M. A. Domingues, M. E. Gomes, *Adv. Healthcare Mater.* **2021**, n/a, 2102076.

[35] D. Wang, W. Zheng, Y. Xie, P. Gong, F. Zhao, B. Yuan, W. Ma, Y. Cui, W. Liu, Y. Sun, M. Piel, W. Zhang, X. Jiang, *Sci. Rep.* **2014**, *4*, 6160.

[36] F. Alisafaei, D. S. Jokhun, G. V. Shivashankar, V. B. Shenoy, *Proc. Natl. Acad. Sci. USA* **2019**, *116*, 13200.

[37] a) A. Totaro, T. Panciera, S. Piccolo, *Nat. Cell Biol.* **2018**, *20*, 888; b) A. R. Tomás, A. I. Gonçalves, E. Paz, P. Freitas, R. M. A. Domingues, M. E. Gomes, *Nanoscale* **2019**, *11*, 18255.

[38] D. Ramos, M. S. Peach, A. D. Mazzocca, X. Yu, S. G. Kumbar, in 8 - Tendon tissue engineering. *Regenerative Engineering of Musculoskeletal Tissues and Interfaces* (Eds: S. P. Nukavarapu, J. W. Freeman, C. T. Laurencin), Woodhead Publishing, Cambridge **2015**, p. 195–217. https://doi.org/10.1016/B978-1-78242-301-0.00008-2.

[39] N. D. Murchison, B. A. Price, D. A. Conner, D. R. Keene, E. N. Olson, C. J. Tabin, R. Schweitzer, *Development* **2007**, *134*, 2697.

[40] Y. Ito, N. Toriuchi, T. Yoshitaka, H. Ueno-Kudoh, T. Sato, S. Yokoyama, K. Nishida, T. Akimoto, M. Takahashi, S. Miyaki, H. Asahara, *Proc. Natl. Acad. Sci. USA* **2010**, *107*, 10538.

[41] H. Yin, M. D. Caceres, Z. Yan, M. Schieker, M. Nerlich, D. Docheva, *Biochem. Biophys. Res. Commun.* **2019**, *512*, 691.

[42] C. Shukunami, A. Takimoto, M. Oro, Y. Hiraki, *Dev. Biol.* **2006**, *298*, 234.

[43] S. Dex, D. Lin, C. Shukunami, D. Docheva, *Gene* **2016**, *587*, 1.

[44] R. Schweitzer, J. H. Chyung, L. C. Murtaugh, A. E. Brent, V. Rosen, E. N. Olson, A. Lassar, C. J. Tabin, *Development* **2001**, *128*, 3855.

[45] D. Docheva, E. B. Hunziker, R. Fässler, O. Brandau, *Mol. Cell. Biol.* **2005**, *25*, 699.

[46] H. R. C. Screen, D. E. Berk, K. E. Kadler, F. Ramirez, M. F. Young, *J. Orthop. Res.* **2015**, *33*, 793.

[47] Y. Bi, D. Ehirchiou, T. M. Kilts, C. A. Inkson, M. C. Embree, W. Sonoyama, L. Li, A. I. Leet, B. M. Seo, L. Zhang, S. Shi, M. F. Young, *Nat. Med.* **2007**, *13*, 1219.

[48] G. Zhang, Y. Ezura, I. Chervoneva, P. S. Robinson, D. P. Beason, E. T. Carine, L. J. Soslowsky, R. V. Iozzo, D. E. Birk, *J. Cell. Biochem.* **2006**, *98*, 1436.

[49] a) C. T. Thorpe, H. L. Birch, P. D. Clegg, H. R. C. Screen, *Int. J. Exp. Pathol.* **2013**, *94*, 248; b) R. T. Kohrs, C. Zhao, Y. L. Sun, G. D. Jay, L.

2102863 (13 of 14)

**ADVANCED
SCIENCE NEWS**

www.advancedsciencenews.com

**ADVANCED
HEALTHCARE
MATERIALS**

www.advhealthmat.de

Zhang, M. L. Warman, K. N. An, P. C. Amadio, *J. Orthop. Res.* **2011**, *29*, 384.

[50] J. Foolen, S. L. Wunderli, S. Loerakker, J. G. Snedeker, *Matrix Biol.* **2018**, *65*, 14.

[51] M. Järvinen, L. Józsa, P. Kannus, T. L. N. Järvinen, M. Kvist, W. Leadbetter, *Scand. J. Med. Sci. Sports* **1997**, *7*, 86.

[52] N. M. Lee, C. Erisken, T. Iskratsch, M. Sheetz, W. N. Levine, H. H. Lu, *Biomaterials* **2017**, *112*, 303.

[53] D. Docheva, S. A. Müller, M. Majewski, C. H. Evans, *Adv. Drug Delivery Rev.* **2015**, *84*, 222.

[54] Y. F. Rui, P. P. Y. Lui, Y. M. Wong, Q. Tan, K. M. Chan, *Stem Cells Dev.* **2013**, *22*, 1076.

[55] C. Zhang, J. Zhu, Y. Zhou, B. P. Thampatty, J. H. C. Wang, *Stem Cells Int.* **2019**, *2019*, 3674647.

[56] W. Bi, J. M. Deng, Z. Zhang, R. R. Behringer, B. de Crombrugghe, *Nat. Genet.* **1999**, *22*, 85.

[57] J. Zhang, J. H. C. Wang, *J. Orthop. Res.* **2010**, *28*, 639.

[58] W. Zhao, X. Wang, K.-H. Sun, L. Zhou, *PLoS One* **2018**, *13*, e0191031.

[59] L. M. Galatz, L. Gerstenfeld, E. Heber-Katz, S. A. Rodeo, *J. Orthop. Res.* **2015**, *33*, 823.

[60] M. de Mos, B. van El, J. DeGroot, H. Jahr, H. T. van Schie, E. R. van Arkel, H. Tol, R. Heijboer, G. J. van Osch, J. A. Verhaar, *Am. J. Sports Med.* **2007**, *35*, 1549.

[61] P. P.-Y. Lui, L.-S. Chan, Y.-W. Lee, S. C. Fu, K.-M. Chan, *Rheumatology* **2010**, *49*, 231.

[62] H. A. Eriksen, A. Pajala, J. Leppilahti, J. Risteli, *J. Orthop. Res.* **2002**, *20*, 1352.

[63] a) S. Tom, J. Parkinson, M. Z. Ilic, J. Cook, J. A. Feller, C. J. Handley, *Matrix Biol.* **2009**, *28*, 230; b) G. P. Riley, M. J. Goddard, B. L. Hazleman, *Rheumatology* **2001**, *40*, 229; c) N. Maffulli, S. W. B. Ewen, S. W. Waterston, J. Reaper, V. Barrass, *Am. J. Sports Med.* **2000**, *28*, 499.

[64] B. R. Seo, X. Chen, L. Ling, Y. H. Song, A. A. Shimpi, S. Choi, J. Gonzalez, J. Sapudom, K. Wang, R. C. Andresen Eguiluz, D. Gourdon, V. B. Shenoy, C. Fischbach, *Proc. Natl. Acad. Sci. USA* **2020**, *117*, 11387.

[65] a) V. J. Thannickal, D. Y. Lee, E. S. White, Z. Cui, J. M. Larios, R. Chacon, J. C. Horowitz, R. M. Day, P. E. Thomas, *J. Biol. Chem.* **2003**, *278*, 12384; b) V. F. Achterberg, L. Buscemi, H. Diekmann, J. Smith-Clerc, H. Schwengler, J. J. Meister, H. Wenck, S. Gallinat, B. Hinz, *J. Invest. Dermatol.* **2014**, *134*, 1862.

[66] Y. D. Shanskii, N. S. Sergeeva, I. K. Sviridova, M. S. Kirakozov, V. A. Kirsanova, S. A. Akhmedova, A. I. Antokhin, V. I. Chissov, *Bull. Exp. Biol. Med.* **2013**, *156*, 146.

[67] a) M. Kjaer, *Physiol. Rev.* **2004**, *84*, 649; b) G. P. Riley, V. Curry, J. DeGroot, B. van El, N. Verzijl, B. L. Hazleman, R. A. Bank, *Matrix Biol.* **2002**, *21*, 185.

[68] M. Tsuzaki, D. Bynum, L. Almekinders, X. Yang, J. Faber, A. J. Banes, *J. Cell. Biochem.* **2003**, *89*, 556.

[69] a) A. Del Buono, F. Oliva, L. Osti, N. Maffulli, *Muscles Ligaments Tendons J.* **2013**, *3*, 51; b) G. Riley, *Nat. Clin. Pract. Rheumatol.* **2008**, *4*, 82.

[70] P. Babo, V. Santo, A. R. C. Duarte, C. Correia, M. H. G. Costa, J. Mano, R. L. Reis, M. E. Gomes, *Inflammation Regener.* **2014**, *34*, 033.

[71] M. C. Echave, R. M. A. Domingues, M. Gómez-Florit, J. L. Pedraz, R. L. Reis, G. Orive, M. E. Gomes, *ACS Appl. Mater. Interfaces* **2019**, *11*, 47771.

[72] R. M. A. Domingues, S. Chiera, P. Gershovich, A. Motta, R. L. Reis, M. E. Gomes, *Adv. Healthcare Mater.* **2016**, *5*, 1364.